Crystal growth, optical spectroscopy, and continuous-wave laser operation of Ho:KLu(WO$_4$)$_2$ crystals

**V. Jambunathan · X. Mateos · M. C. Pujol ·
J. J. Carvajal · C. Zaldo · U. Griebner ·
V. Petrov · M. Aguiló · F. Díaz**

Abstract We present the crystal growth, optical spectroscopy, and room temperature continuous-wave (CW) laser operation of monoclinic Ho:KLu(WO$_4$)$_2$ crystals. Macro defect-free crystals of several dopant concentrations were grown by top-seeded solution growth slow-cooling method. The evolution of unit cell parameters with holmium doping level and temperature was studied using X-ray powder diffraction. The spectroscopic properties were characterized in terms of room- and low-temperature optical absorption and photoluminescence. From low-temperature optical absorption measurements, the energy of the Stark levels was determined. Calculation of the emission and gain cross sections is presented. CW laser action was realized for 3 and 5 at. % Ho-doped KLu(WO$_4$)$_2$ by in-band pumping using a Tm:KLu(WO$_4$)$_2$ pump laser. A maximum output power of 507 mW with a slope efficiency of ∼38 % with respect to the incident power was achieved at 2,080 nm with the Ho:KLu(WO$_4$)$_2$ laser.

V. Jambunathan · X. Mateos (✉) · M. C. Pujol ·
J. J. Carvajal · M. Aguiló · F. Díaz
Física i Cristal·lografia de Materials i Nanomaterials
(FiCMA-FiCNA), Universitat Rovira i Virgili (URV), Campus
Sescelades c/Marcel·lí Domingo, s/n, 43007 Tarragona, Spain
e-mail: xavier.mateos@urv.cat

X. Mateos · U. Griebner · V. Petrov
Max-Born Institute for Nonlinear Optics and Short Pulse
Spectroscopy, Max-Born Strasse 2A, 12489 Berlin, Germany

C. Zaldo
Instituto de Ciencia de Materiales de Madrid, Consejo Superior
de Investigaciones Científicas, c/Sor Juana Inés de la Cruz 3,
28049 Madrid, Spain

1 Introduction

Infrared ∼2 µm eye-safe lasers based on active lanthanide ions are of current interest because of their vast demand in scientific and technological applications, for example in medicine, remote sensing, and as a pump source for optical parametric oscillator (OPO) systems [1–4]. Efficient lanthanide-based ∼2 µm infrared solid-state lasers can be accomplished by Ho^{3+} ions due to large transition (absorption and emission) cross sections and long lifetime of the ^{5}I$_7$ manifold. The main limitation of Ho lasers is related to the pump mechanism, and the availability of suitable pump sources can substitute flash lamps. For this, many authors used another Tm^{3+}, to sensitize the Ho emission through energy transfer while conveniently pumping the Tm ions with commercial, powerful, and compact diode lasers operating around 808 nm [5, 6]. However, non-perfect energy resonance between energy levels and up-conversion processes reduces the laser efficiency in such co-doped laser systems. A second approach, in order to increase the laser efficiency and the output power, is to excite the Ho ions directly to the emitting level (^{5}I$_7$), the so-called in-band or resonant pumping using another ∼2 µm laser operating at slightly shorter wavelength. Both bulk and fiber Tm lasers are very suitable for this since they emit in general at shorter wavelengths (depending on the host) that are suitable to match the absorption curve of Ho in this spectral range [7–12]. The great advantage of this strategy is the drastic reduction in the energy difference between the pump and laser photons, the so-called quantum defect, allowing power scaling with less thermal problems.

Concerning the host for the active ion, the monoclinic double tungstate crystals, KRE(WO$_4$)$_2$ (RE = Y, Gd, Lu), are very suitable for solid-state lasers when doped with

lanthanides, as proved recently for the Yb and Tm ions [13]. These crystals stand out because of the large transition cross sections and the possibility of high doping levels, up to 100 % as demonstrated previously [14]. Bearing all this in mind, our work focused on the crystal growth of a series of single-doped Ho:KLuW crystals, their spectroscopic characterization, and laser performance under resonant pumping using Tm:KLuW laser as pump source [15].

2 Experimental

Ho:KLuW crystals with several Ho concentrations were grown by the top-seeded method using $K_2W_2O_7$ as solvent. The detailed methodology of growth is described in [16]. The raw reagents were from Aldrich, Fluka and Metall rare-earth Ltd., with analytical grade of purity. The chemical composition of the grown single crystals was measured using an electron probe microanalyzer (EPMA). X-ray powder diffraction was used to study the evolution of the unit cell parameters with doping level (carried out with a Bruker-AXSD8-Discover diffractometer) and with temperature (carried out with a Siemens D-5000 diffractometer).

For the spectroscopic characterization, taking into account the remarkable physical anisotropy of the KLuW crystal, the samples were cut and polished perpendicular to the principal optical directions, designated as N_g, N_m, and N_p (defined by the values of the refractive indexes, $n_g > n_m > n_p$) to study their behavior depending on the polarization of the incident light. The polarized room- and low-temperature optical absorption measurements were taken using a Glan–Thomson polarizer in front of the sample and were recorded in the 300–2,400 nm range with a Cary Varian 500 spectrophotometer. To lower the temperature, a cryostat from Oerlikon Leybold Vacuum GmbH (coolpak 6000 model) with a liquid helium closed circuit was used. Room- and low-temperature photoluminescence measurements of the Ho:KLuW crystal were taken by exciting the crystal using an OPO system (Opotek, model Vibrant HE 355II + UV). The detection was at an angle of 90° with respect to the incident beam in order to avoid the influence of the pump. The emission signals were collected and dispersed through a 460-mm Jobin–Yvon monocromator using a 300 groves/mm diffraction grating. For the detection of the signal, we used a InAs-based detector cooled down to liquid nitrogen temperature (77 K), connected to a preamplifier and to a lock-in amplifier. The intensity decay of the fluorescence was measured after excitation with a Quanta-Ray MOPO system, and the fluorescence was dispersed by a 340-mm single-grating SPEX spectrophotometer, detected by a cooled InSb detector and recorded in a Tektronix digital oscilloscope (TDS-520).
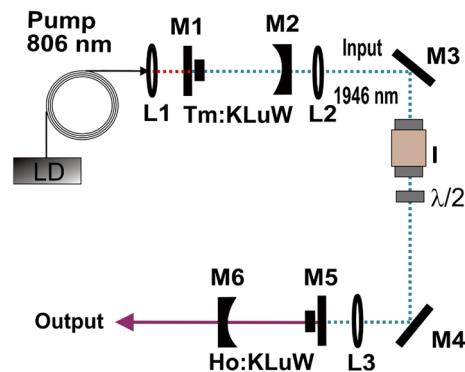
Fig. 1 Laser setup of the Ho:KLuW laser

Laser operation was studied by a simple hemispherical resonator as shown in Fig. 1. It comprises a plane mirror (M5) that was antireflection-coated for the pump wavelength in the 1,900–1,970 nm range and high reflection-coated for the laser wavelength in the 2,000–2,100 nm range and a curved output coupler (M6) with a radii of curvature of 50 mm and transmission of 1.5 (±0.3), 3 (±0.5), 5 (±1.0), and 20 (±4.0) % in the 1,820–2,050 nm range. For focusing the pump beam onto the Ho:KLuW sample, we used a 50-mm focal length lens (L3). The active elements of 3 and 5 at. % Ho:KLuW were mounted in a Cu holder and wrapped in In foil for better thermal contact with the holder (water-cooled to 16 °C) at the top and bottom surface of the sample. The samples were antireflection-coated for pump and laser wavelength in a broad range from 1,900 to 2,200 nm, and placed as close as possible to the pump mirror with the orientation for light propagation along N_g. The thickness of the samples was 3 mm, and the aperture was 3×3 mm^2. The pump source was a diode-pumped Tm:KLuW laser described elsewhere [15]. Its emission spectrum was centered at 1,946 nm with a maximum output power of 4.0 W. The emission from the Tm:KLuW was linearly polarized along its N_m principal axis. In order to avoid back coupling from the Ho-laser cavity, we used an optical isolator. A half-wave plate after the isolator was used to convert the pump polarization to vertical.

3 Results and discussion

3.1 Crystal growth

Defect-free Ho:KLuW single crystals with several Ho concentrations were grown by the TSSG–SC method. These were (in atomic percentage in the solution) 0.5, 1.0, 3, 5, and 7.5 at. %, where the active Ho ions substitute for the Lu ions in the structure. To grow the single crystals, 200 g of the solution mixture was inserted in a platinum

crucible, 50 mm in diameter and 50 mm in height. The mixture was composed of proper amounts of K_2CO_3, Ho_2O_3, WO_3, and Lu_2O_3 reagents. The solution composition was 12 mol. % KLuW as solute—88.0 mol. % $K_2W_2O_7$ as solvent because previous studies of the solubility curves [17] confirmed that this ratio with low solute content is optimum to produce steep changes in the saturation temperature with the composition as well as to enable growing of high-quality crystals.

The filled crucible was introduced in a vertical tubular furnace so that the mixture was homogenized 50 K above the saturation temperature for about 7–8 h. The thermal axial gradient measured in the solution was maintained around $\sim$1.5 K/cm. To favor nucleation, a crystallographic b-oriented KLuW seed was used and located at the center of the surface of the homogeneous solution. The saturation temperature was determined by accurate observation of the growth and/or dissolution of the seed. The solution temperature was then decreased by about 20 K at a rate of 0.1–0.15 K/h while the seed was rotated at 40 rpm in order to enhance the mass and heat transfer to the growing crystal. After approximately 8–10 days of growth, the crystals were slowly removed from the solution at the rate of 1 mm/10 min and after losing contact with the solution, the furnace was cooled down to room temperature at a rate of 25 K/h to avoid cracking of the crystals caused by abrupt change in temperature. The dimensions of the grown crystals ranged typically from 17.13 to 20.84 mm, from 9.85 to 10.16 mm, and from 6.87 to 7.71 mm for c, $a*$ and b directions, respectively. Figure 2 shows photography of 1 at. % Ho:KLuW crystal as an example. The weight of the crystals was in the range of 4.5–5.5 g. The

Fig. 2 Photograph of 1 at. % Ho:KLuW crystal
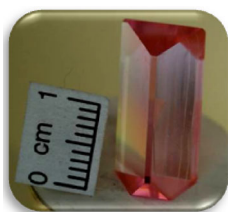
growth rate varied from 231 to 24 $\times 10^{-4}$ g/h. The saturation temperature was between 1,158 and 1,168 K. Table 1 summarizes all these parameters for each of the grown crystals, as well as the ion density measured in the crystals, thus giving the stoichiometric formula.

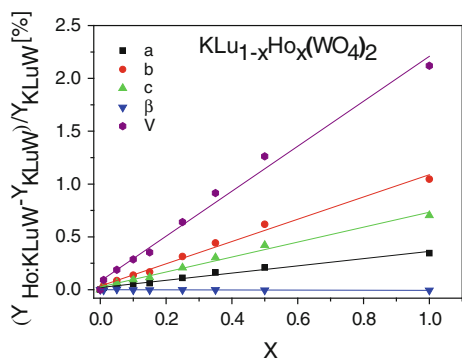### 3.2 Evolution of unit cell parameters with the doping level and temperature

The Ho:KLuW crystal shows a morphology similar to that of un-doped KLuW [18]. The study of the evolution of the unit cell parameters with the doping concentration is of great interest to know how the structure is modified when the doping concentration increases, since a priori the optimum doping level for infrared laser operation is unknown. Furthermore, under high pump laser power conditions, the active medium is heated producing mechanical stress due to anisotropic thermal expansion. Hence, the evolution of the unit cell parameters with temperature is important for scaling the output power of the laser.

We first studied the evolution of the unit cell parameters with Ho-doping level using 1, 5, 10, 15, 25, 35, 50, and 100 at. %). These were calculated by fitting with the FULLPROF software [19], and the X-ray powder diffraction patterns were obtained with $2\theta = 5°–70°$ with step size of 0.02° and step time of 16 s. Figure 3 shows the evolution of unit cell parameters with the doping level of Ho in the structure. We conclude that there is an increase in the unit cell parameters a, b, and c; however, β (the angle between a and c directions) remains basically constant. The reason for this expansion is that the ionic radius of Ho^{3+} (1.015 Å) is slightly larger than that of the substituted Lu^{3+} (0.977 Å) (values taken from [20] for coordination number 8).

To determine the linear thermal expansion tensor, the unit cell parameters of 3 at.% Ho:KLuW crystal powder were measured as a function of temperature (at 303, 323, 373, 473, 573, 673, 773, 873 K) and by fitting with the FULLPROF software, the X-ray power diffraction patterns were obtained with $2\theta = 10°–70°$, step size of 0.03° and step time of 5 s. Figure 4 shows the evolution of unit cell

Table 1 Summary of the crystal grown experiments, the concentrations determined by EPMA, and the stoichiometric formula

at. % of Ho^{3+}	Cooling rate (K/h)	Cooling interval (K)	Crystal weight (g)	Growth rate [$\times 10^{-4}$] (g/h)	Crystal dimensions along the crystallographic directions (mm)			Saturation temperature (K)	Ho^{3+} in KLuW (at./cm^3)	Stoichiometric formula
					c	$a*$	b			
0.5	0.10	24.0	5.5	231	18.43	9.85	7.71	1,158.3	5.456×10^{19}	$KLu_{0.992}Ho_{0.008}(WO_4)_2$
1.0	0.10	20.0	4.8	242	19.13	10.16	6.87	1,157.9	9.307×10^{19}	$KLu_{0.986}Ho_{0.014}(WO_4)_2$
3.0	0.10	21.2	4.9	230	20.84	10.07	6.90	1,166.5	2.543×10^{20}	$KLu_{0.961}Ho_{0.039}(WO_4)_2$
5.0	0.10/0.15	17.0/3.0	4.5	238	17.13	10.03	7.30	1,167.8	4.119×10^{20}	$KLu_{0.937}Ho_{0.063}(WO_4)_2$
7.5	0.10/0.15	16.5/3.5	4.6	243	17.64	9.96	7.26	1,164.9	5.246×10^{20}	$KLu_{0.920}Ho_{0.080}(WO_4)_2$

Fig. 3 Evolution of unit cell parameters and volume V of Ho:KLuW with doping concentration
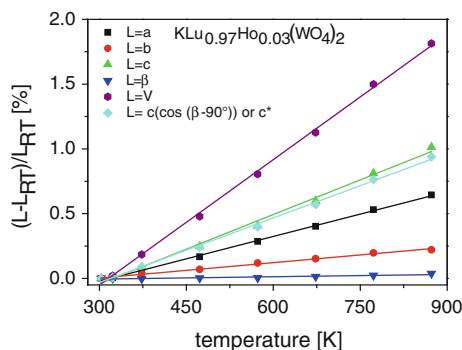
Fig. 4 Evolution of unit cell parameters and volume V with temperature

parameters versus temperature. It can be seen that the unit cell parameters increase with temperature while β remains basically constant.

The values of the linear thermal expansion coefficients are obtained from the slopes of the linear relationship between the change in $\Delta L/L$ (L: a, b, c, c^*, and V) and the temperature along the crystallographic directions. The results for the 3 at. % Ho:KLuW are $\alpha_a = 11.5 \times 10^{-6}$ K^{-1}, $\alpha_b = 3.98 \times 10^{-6}$ K^{-1}, $\alpha_c = 17.8 \times 10^{-6}$ K^{-1}, $\alpha_{c*} = 16.6 \times 10^{-6}$ K^{-1}, $\alpha_v = 32.2 \times 10^{-6}$ K^{-1}.

The linear thermal expansion tensor at room temperature in the orthogonal crystallophysical system $X_1//a$, $X_2//b$, $X_3//c^*$ is
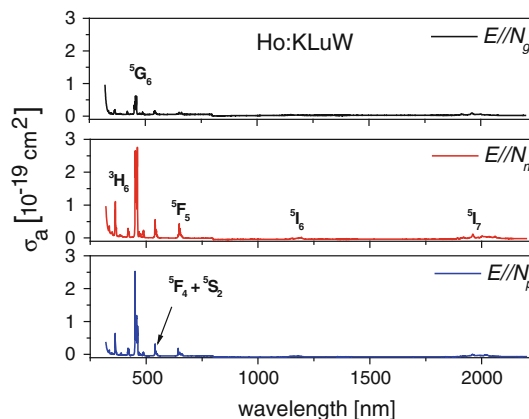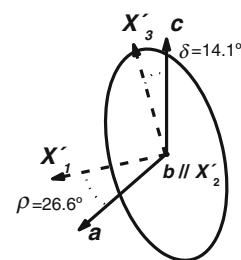
$$\alpha_{ij} = \begin{pmatrix} 11.5 & 0 & -3.41 \\ 0 & 3.98 & 0 \\ -3.41 & 0 & 16.6 \end{pmatrix} \times 10^{-6} \text{ K}^{-1}$$

and in its principal (Eigen) frame X_1', $X_2'//b$, X_3', it has the form:

$$\alpha_{ij}' = \begin{pmatrix} 9.79 & 0 & 0 \\ 0 & 3.98 & 0 \\ 0 & 0 & 18.31 \end{pmatrix} \times 10^{-6} \text{ K}^{-1}$$

The principal axis with maximum thermal expansion, X_3', is found at 14.1° anticlockwise rotation from the c

Fig. 5 Thermal expansion ellipsoid of 3 at. % Ho:KLuW

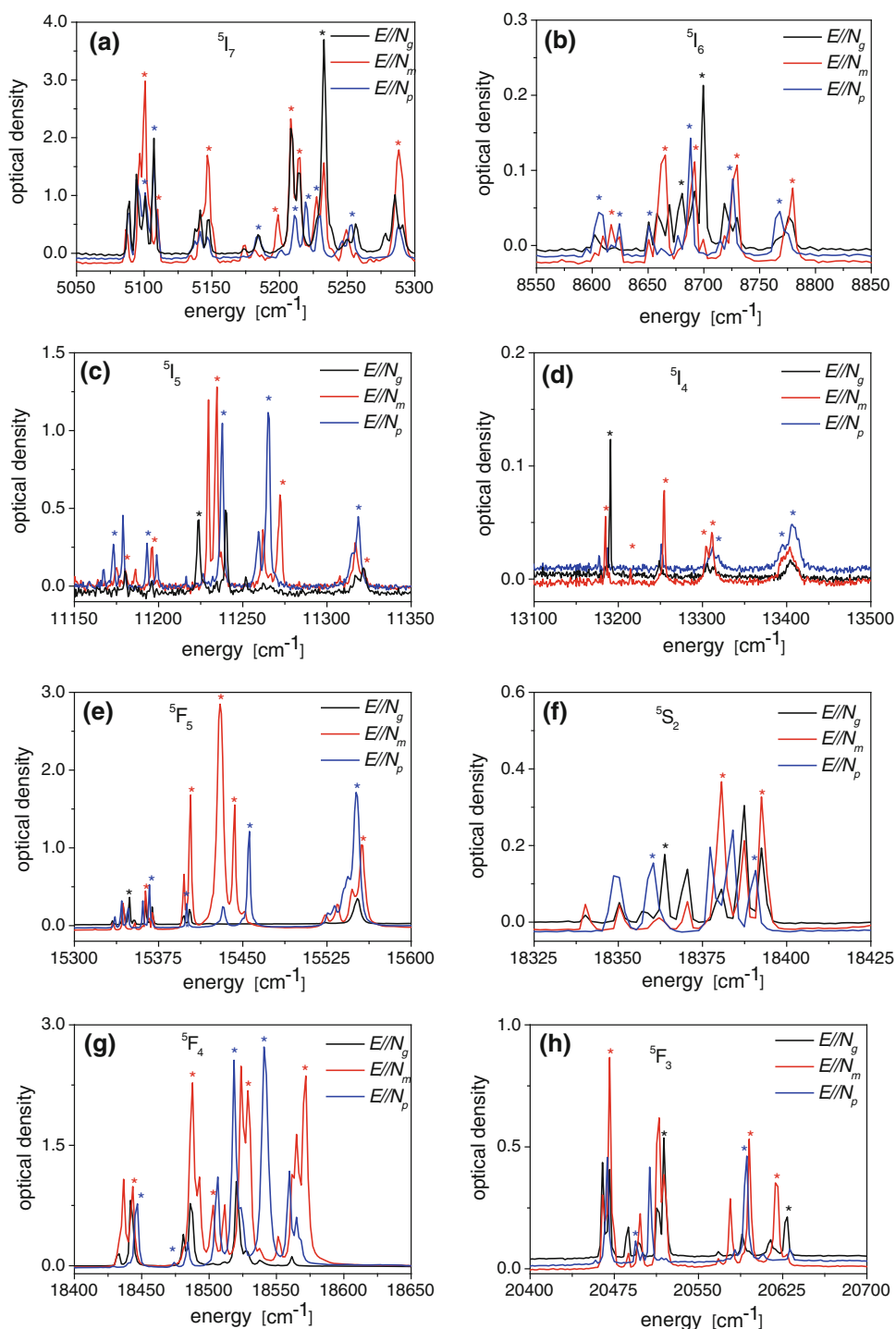**Fig. 6** Polarized room temperature absorption cross section of Ho:KLuW crystal in the 300–2,200 nm range

crystallographic axis with the positive b axis pointing toward the observer, and the principal axis with medium thermal expansion X_1' is at 26.6° clockwise from the a crystallographic axis. The thermal expansion ellipsoid for 3 at. % Ho:KLuW is shown in Fig. 5. The thermal expansion results are in agreement with those obtained for undoped KLuW [18].

3.3 Optical absorption

Polarized optical absorption at room temperature of holmium in KLuW host was measured using the cut and polished crystals as mentioned earlier. We considered 1 at. % Ho-doped sample with a concentration of 9.307×10^{19} at./cm^3, and thickness of 2.91 mm along N_p and 2.71 mm along N_g axes. These concentration and thickness were suitable to get a noise-free signal and also to avoid saturation of the detectors. Figure 6 shows the polarized room temperature absorption cross section of the Ho:KLuW crystal in the 300–2,200 nm spectral range. Strong anisotropy can be observed. Polarization parallel to N_m shows generally the highest values of absorption cross section. Around 450–460 nm, the $^5G_6$ level has the highest absorption cross section with a value of $\sim 2.7 \times 10^{-19}$ cm^2.

The splitting of different manifolds is in agreement with their multiplicity. In low-temperature

Fig. 7 a–q Low-temperature (6 K) optical absorption of KLuW single crystal doped with holmium and recorded with light polarized parallel to the three principal optical directions N_g, N_m, and N_p

measurements, the extra peaks caused by thermal population of various sublevels of the ground state and possible vibronic peaks were eliminated. Figure 7a–q shows the polarized low-temperature absorption spectra of each excited state from ground state and * indicates the electronic transitions between the different sublevels. These experimentally determined sublevels are in agreement with the splitting by the crystal field observed for the similar Ho:KGdW crystal [21]. Table 2 shows 171 Stark levels of Ho^{3+} in KLuW. The peaks are assigned by comparing the intensity of each of the polarizations N_g, N_m, and N_p. Also, it should be mentioned that in Table 2, the labels not in parentheses indicate the polarization character of every peak and those in parentheses indicate the contribution of other polarizations for that peak.

Fig. 7 continued
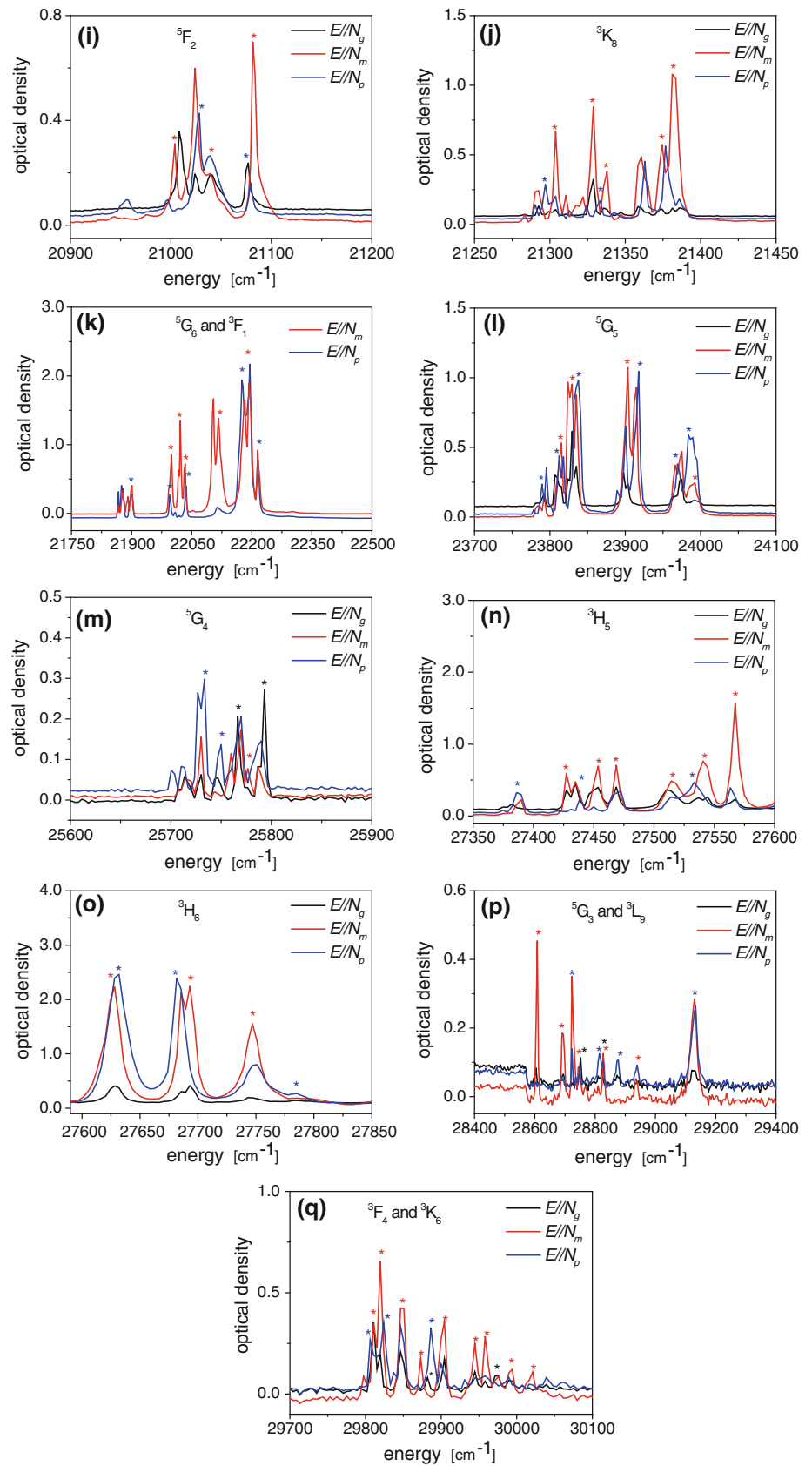
Table 2 Experimental energy levels, E_{exp} (in cm^{-1}) and polarization label, $E//N_{g,p,m}$, of Ho^{3+} ions in the KLuW single crystal

$^{2s+1}L_J$	$E//N_{g,m,p}$	E_{exp} (cm^{-1})
$^5I_7$	m	5,100
	$p(g)$	5,101
	$p(g)$	5,107
	$mg(p)$	5,109
	$mg(p)$	5,147
	$p(g)$	5,184
	m	5,199
	mg	5,208
	p	5,211
	mg	5,214
	p	5,219
	p	5,230
	$g(m)$	5,233
	p	5,253
	$m(p)$	5,288
$^5I_6$	$p(mg)$	8,607
	$m(p)$	8,618
	$p(m)$	8,624
	$p(g)$	8,651
	mg	8,663
	g	8,680
	p	8,687
	mg	8,690
	gm	8,699
	p	8,726
	mg	8,728
	p	8,766
	mg	8,778
$^5I_5$	p	11,173
	$mg(p)$	11,180
	p	11,193
	mg	11,196
	g	11,225
	m	11,235
	$p(g)$	11,238
	p	11,259
	m	11,272
	$p(mg)$	11,319
	mg	11,321
$^5I_4$	m	13,185
	g	13,191
	m	13,214
	$mg(p)$	13,254
	m	13,305
	$mg(p)$	13,314
	p	13,319
	$p(mg)$	13,394
	$p(mg)$	13,407

Table 2 continued

$^{2s+1}L_J$	$E//N_{g,m,p}$	E_{exp} (cm^{-1})
$^5F_5$ 1 peak missing	$g(p)$	15,349
	mg	15,364
	p	15,367
	p	15,400
	mg	15,403
	m	15,430
	m	15,442
	p	15,456
	$p(g)$	15,552
	m	15,556
$^5S_2$	p	18,360
	g	18,364
	mg	18,381
	p	18,390
	mg	18,393
$^5F_4$	mg	18,442
	p	18,446
	p	18,474
	mg	18,488
	m	18,503
	p	18,518
	m	18,528
	p	18,541
	m	18,572
$^5F_3$	mg	20,471
	p	20,495
	$g(m)$	20,520
	$p(g)$	20,593
	m	20,595
	m	20,620
	$g(p)$	20,629
$^5F_2$	m	21,004
	p	21,028
	$gm(p)$	21,040
	p	21,079
	m	21,083
$^3K_8$ 10 peaks missing	p	21,297
	$mg(p)$	21,304
	mg	21,329
	p	21,333
	mg	21,338
	m	21,374
	m	21,382
$^5G_6$ and $^5F_1$ 6 peaks missing	$p(m)$	21,900
	p	21,966
	m	21,999
	m	22,022
	m	22,032

Table 2 continued

$^{2s+1}L_J$	$E//N_{g,m,p}$	E_{exp} (cm^{-1})
	p	22,035
	m	22,115
	$p(m)$	22,177
	$m(p)$	22,194
	$p(m)$	22,218
$^5G_5$	p	23,789
1	$p(g)$	23,812
peak missing	mg	23,815
	mg	23,830
	p	23,837
	mgp	23,903
	$p(m)$	23,918
	$p(mg)$	23,967
	p	23,984
	$m(p)$	23,994
$^5G_4$	$p(mg$	25,734
4 peaks missing	$p(g)$	25,747
	$g(mp)$	25,767
	mg	25,776
	$g(mp)$	25,794
$^3H_5$	$p(m)$	27,387
2 peaks missing	mg	27,427
	$p(mg)$	27,439
	mg	27,453
	$mg(p)$	27,469
	$mg(p)$	27,515
	$p(g)$	27,533
	mg	27,541
	$mg(p)$	27,567
$^3H_6$	m	27,627
7 peaks missing	$p(g)$	27,631
	p	27,681
	mg	27,694
	$mg(p)$	27,747
	p	27,783
G_3 and $^3L_9$	mg	28,607
15 peaks missing	$mg(p)$	28,693
	$p(m)$	28,725
	$m(p)$	28,746
	g	28,751
	p	28,816
	g	28,822
	m	28,828
	$p(g)$	28,875
	$m(p)$	28,937
	$p(mg)$	29,129

Table 2 continued

$^{2s+1}L_J$	$E//N_{g,m,p}$	E_{exp} (cm^{-1})
$^3F_4$ and $^3K_6$	p	29,807
8 peaks missing	mg	29,811
	mg	29,821
	p	29,823
	$mg(p)$	29,848
	m	29,873
	g	29,881
	p	29,887
	$mg(p)$	29,902
	$mg(p)$	29,944
	$m(p)$	29,959
	$g(m)$	29,975
	$mg(p)$	29,991
	m	30,020
$^5I_8$		0
2 peaks missing	$+$	4
	$+$	6
	$+$	11
	$+$	21
	$+$	32
		43
		62
		106
		118
		144
		183
		209
		250
		292

The energy values of the Stark levels have been experimentally obtained by optical absorption and for the ground state ($^5I_8$), by photoluminescence measurements at 6 K

$+$ extra peaks observed in the low-temperature absorption measurement

3.4 Photoluminescence

The objective of the photoluminescence experiments was to determine the emission properties of Ho at room temperature around 2 μm and also to determine the energy sublevels of the ground state ($^5I_8$ state) from low-temperature emission measurements. The photoluminescence measurements were obtained with a 1 at. % Ho:KLuW crystal with a concentration of 9.307×10^{19} at./cm^3, excited at 454 nm (22,000 cm^{-1}). This level was chosen for exciting the crystal for luminescence experiments because the absorption cross section was higher compared
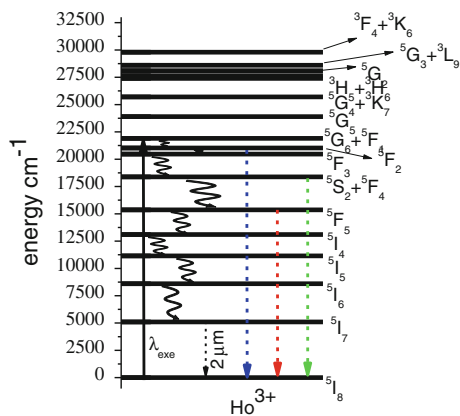
Fig. 8 Energy level diagram of Ho^{3+} in KLuW
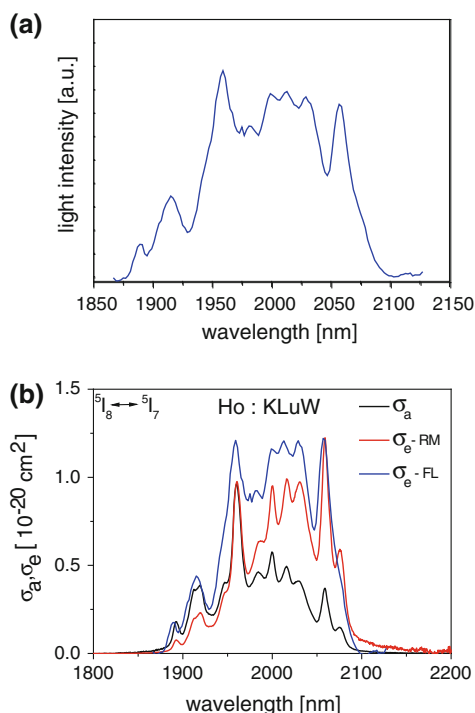

Fig. 9 a Unpolarized emission spectrum of 5 at. % Ho:KLuW in the 2 μm spectral range. **b** Calculated emission cross section using the reciprocity (*red*) and the Füchtbauer–Ladenburg (*blue*) methods

to the other levels as mentioned earlier. After excitation, several de-excitation processes take place radiatively and non-radiatively as shown in the energy level diagram of Fig. 8. We observed several emissions in the blue, green, red, and in the infrared near 2 μm, but we focused on the last one that is responsible for the laser operation studied later. From the low-temperature emission around 2 μm ($^5I_7 \rightarrow {}^5I_8$) and 550 nm ($^5S_2 \rightarrow {}^5I_8$), we determined the Stark level energies of the ground state $^5I_8$ (see Table 2). Figure 9a shows the unpolarized 2 μm measured emission spectrum and as can be seen, it consists of the overlapping of several bands extending from ~1,850 to ~2,100 nm.

The important parameter that defines the laser performance of a material is the emission cross section. It can be calculated by the reciprocity method (RM) [22], which makes use of the experimental absorption cross section, and by the Füchtbauer–Ladenburg (FL) [22] method, which makes use of the experimental emission data and the radiative lifetime. To quantify and to compare the shape of the experimental photoluminescence from Ho^{3+} around 2 μm, we first measured the optical absorption in the 1,800–2,200 nm range of single-doped 5 at. % Ho:KLuW crystal with light polarized parallel to the three principal optical directions, N_g, N_m, and N_p. Then, by using the RM method, we calculated the polarized emission cross sections and averaged the results with respect to the polarization in order to compare with the unpolarized experimental photoluminescence. We also calculated the emission cross section with the FL method using the emission spectrum shown in Fig. 9a and the $^5I_7$ fluorescence lifetime measured in the next section for the 1 at. % Ho-doping level.

Figure 9b shows the polarization-averaged absorption and the calculated emission cross sections using the RM and FL methods. The shape of the emission spectra obtained is similar for the two methods, and the quantified emission cross section matches exactly at 2,060 nm with a value of ~1.22×10^{-20} cm^2.

The knowledge of the polarization dependence of the emission and gain cross sections is important in order to predict and compare with the naturally selected polarization in laser operation. Figure 10a–c shows the polarized absorption and calculated emission cross sections of Ho:KLuW using the RM for $E//N_g$, N_m, and N_p principal optical directions. From the figures, one obtains a maximum emission cross section of ~0.76×10^{-20} cm^2 for $E//N_g$ at 2,000 nm, ~2.42×10^{-20} cm^2 for $E//N_m$ at 2,060 nm and ~1.29×10^{-20} cm^2 for $E//N_p$ at 2,017 nm.

The gain cross section σ_g was computed with the following expression:

$$\sigma_g = \sigma_e \times \beta - (1 - \beta) \times \sigma_a$$

where β is the population inversion level.

Figure 11a–c shows the calculated gain cross section for $E//N_g$, N_m, and N_p principal optical directions, respectively. From the figures, it is inferred that for a population inversion level of 0.5, positive gain is expected for wavelengths exceeding 1,960 nm. In contrast to Tm:KLuW [15], where the gain cross section obviously predicts some polarization competition between $E//N_p$ and N_m (also observed experimentally [23]), from Fig. 11, it is obvious that $E//N_m$ will be the polarization naturally selected by Ho:KLuW the laser.
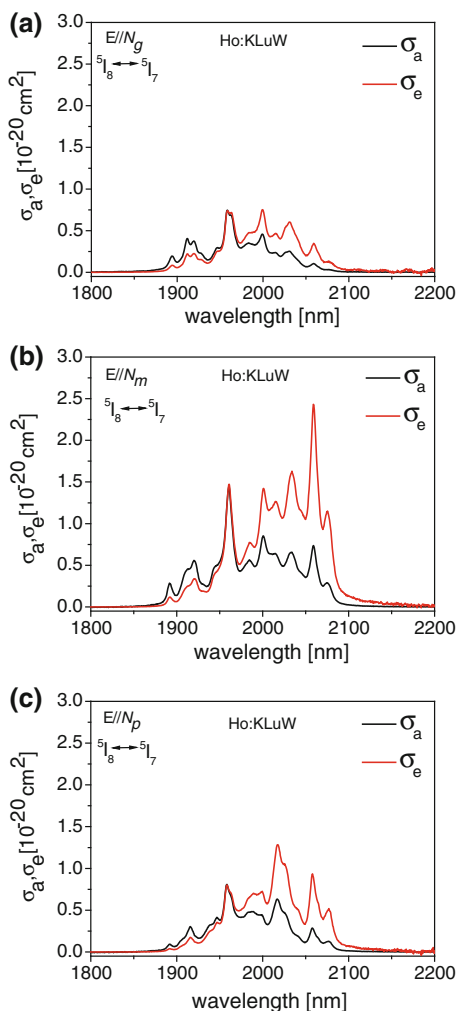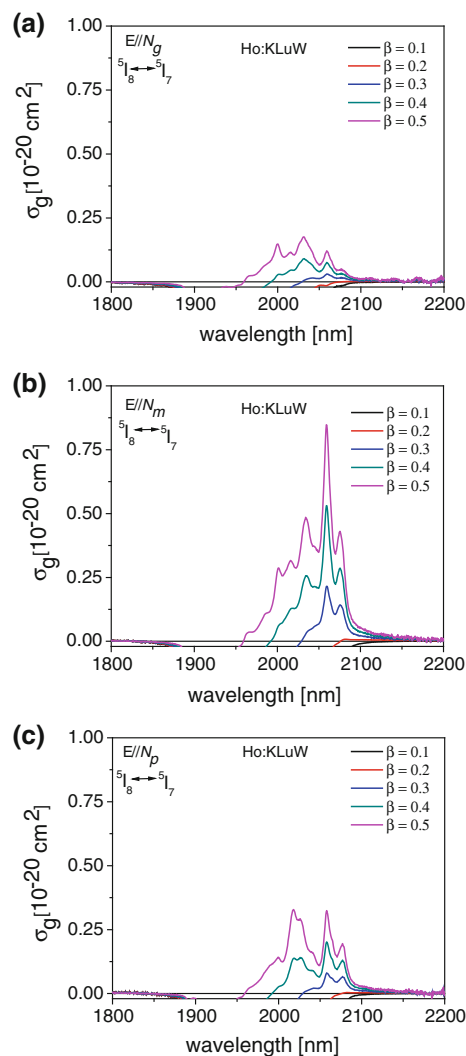
Fig. 10 a–c Polarized absorption cross section and calculated emission cross section for $E//N_g$, N_m, and N_p principal optical directions in Ho:KLuW

3.5 Fluorescence decay time measurements

The temporal decay of the fluorescence intensity was measured by exciting Ho:KLuW samples through the $^5I_6$ ($\lambda = 1{,}175$ nm) or through the $^5I_5$ ($\lambda = 914$ nm) Ho^{3+} multiplets. In both cases, the emission wavelength was 2,050 nm and the decay curves were observed on a digital oscilloscope. We measured the lifetime for different concentrations, 1, 3, and 5 at. % of Ho. The results, not shown for the sake of brevity, were in all cases well fitted by a single exponential. The data obtained are summarized in Table 3.

From Table 3, it can be concluded that the increased lifetime in the case of 3 and 5 at. % Ho-doping is due to emission re-absorption. In order to estimate the deviation of these experimentally determined decay constants from true lifetime values, we can estimate the radiative lifetime


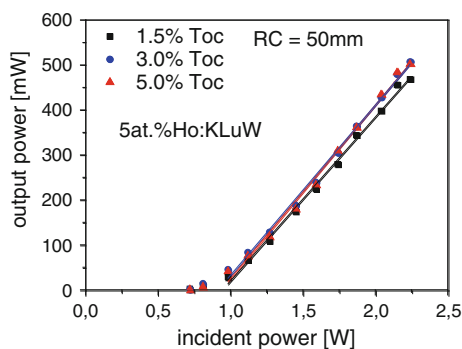**Fig. 11 a–c** Calculated gain cross section for $E//N_g$, N_m, and N_p principal optical directions in Ho:KLuW

Table 3 Fluorescence decay time measurement at 2,050 nm in Ho:KLuW crystals

at. % Ho	λ_{exc} (nm)	τ (ms)	λ_{exc} (nm)	τ (ms)
1	1,175	5.5	914	5.8
3	1,175	8.4	914	8.4
5	1,175	7.8	914	9.2

of Ho in KLuW. For this purpose, we used FL method in a reverse way, taking into account a polarization average value of the emission cross section calculated from those obtained by the RM and the partition functions calculated from the energy levels in Table 2. We estimate a $^5I_7$ radiative lifetime of 5.38 ms, which almost matches with the measured lifetime for the 1 at. % Ho-doping level.
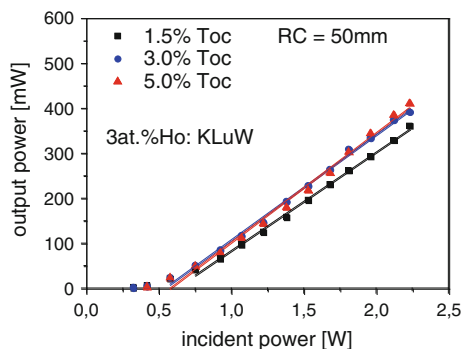
Fig. 12 Output power versus incident pump power for the 3 at. % Ho:KLuW laser

Fig. 13 Output power versus incident pump power for the 5 at. % Ho:KLuW laser

Table 4 Summary of the laser results obtained with 3 and 5 at. % Ho:KLuW for different output coupling T_{oc}, P_{out}: maximum output power, η: slope efficiency with respect to incident pump power, P_{th}: laser threshold, λ: laser wavelength

Sample	T_{oc} (%)	P_{out} (mW)	η (%)	P_{th} (mW)	λ (nm)
3 % Ho:KLuW	1.5	361	21.9	323	2,080
	3.0	392	23.4	323	2,079
	5.0	411	24.3	417	2,077
5 % Ho:KLuW	1.5	468	36.4	720	2,080
	3.0	507	37.9	720	2,080
	5.0	502	38.6	720	2,078

3.6 Laser experiments

Laser experiments were carried out with the setup described in the experimental section. CW laser action was realized for the 3 and 5 at. % N_g-cut Ho:KLuW. In all cases, the incident power was limited to 2.3 W in order to avoid damage of the active media since the pump spot diameter was of the order of 130 μm. In the absence of polarization selective elements, the Ho:KLuW laser naturally selected the $E//N_m$ polarization, which exhibits higher gain than the $E//N_p$ polarization according to the spectroscopic results.

Figures 12 and 13 show the input–output characteristics of the 3 and 5 at. % Ho:KLuW lasers, respectively, using output couplers of transmission $T_{oc} = 1.5$, 3 and 5 %. The physical cavity length was 50 ± 1 mm, and double pump pass scheme was employed through the output coupler that made it difficult to estimate the crystal absorption under lasing conditions.

In general, considerably higher pump efficiency was obtained in comparison with our initial laser work with uncoated Ho:KLuW samples [24]. Comparing the results in Figs. 12, 13, and Table 4 one can infer that 5 at. % Ho:KLuW gives higher slope efficiency than 3 at. % Ho-doping.

No saturation of the power dependence can be seen in Figs. 12 and 13, which means that thermal load is still not an issue at these powers levels. Thus, considerable improvement in the output power can be expected by using other pump sources and different cavity designs.

Also, one can observe a shift toward shorter laser wavelengths in both cases with the increase in the transmission of the output coupler (see Table 4). This is typical for quasi-three-level laser systems. The shift in wavelength is in accordance with the gain curve in Fig. 11b where the transition takes place between $\beta = 0.2$ and 0.3.

The laser threshold (Table 4) for different couplers is unusually similar in some cases as, for example, with 5 at. % Ho:KLuW. The explanation for this is that the step to increase the current applied to the pump diode is fixed by the power supply. This means that below a certain current level, the Ho laser does not reach the laser threshold and for one step more of the current level, threshold is reached for the three coupler transmissions.

4 Conclusions

We have grown macro defect-free Ho:KLuW crystals with different dopant concentrations by the TSSG–SC method. These crystals were structurally, compositionally, and spectroscopically characterized. The highest emission cross section is observed for light polarized parallel to the N_m optical axis. Continuous-wave laser operation was studied at room temperature using 3 and 5 at. % Ho:KLuW crystals in-band pumped by a Tm:KLuW laser. The Ho:KLuW laser delivered maximum output power of ~ 500 mW with a slope efficiency of ~ 38 % with respect to the incident pump power, at a wavelength of $\sim 2,080$ nm. Present results encourage future work on the power scaling of these infrared lasers using diode lasers as pump sources with optimized doping levels, thickness, and pump wavelength.

References

1. S. Pierre, G.M. Preminger, World J. Urol. **25**, 235 (2007)
2. R. Targ, M.J. Kavaya, R.M. Huffaker, R.L. Bowles, Appl. Opt. **30**, 2013 (1991)
3. S.W. Henderson, C.P. Hale, J.R. Magee, M. Kavaya, A.V. Jand Huffaker, Opt. Lett. **16**, 773 (1991)
4. P.A. Budni, L.A. Pomeranz, M.L. Lemons, C.A. Miller, J.R. Mosto, E.P. Chicklis, J. Opt. Soc. Am. B **17**, 723 (2000)
5. V. Sudesh, K. Asai, J. Opt. Soc. Am. B **20**, 1829 (2003)
6. A. Sato, K. Asai, K. Mizutani, Opt. Lett. **29**, 836 (2004)
7. R.C. Stoneman, L. Esterowitz, Opt. Lett. **17**, 736 (1992)
8. S. So, J.I. Mackenzie, D.P. Shepherd, W.A. Clarkson, J.G. Betterton, E.K. Gorton, J.A.C. Terry, Opt. Express **14**, 0481 (2006)
9. D. Xiao-Ming, Y. Bao-Quan, Z. Yun-Jun, S. Cheng-Wei, G. Jing, J. You-Lun, W. Yue-Zhu, Chin. Phys. Lett. **25**, 1693 (2008)
10. B.Q. Yao, L.L. Zheng, R.L. Zhou, X.M. Duan, Y.J. Zhang, Y.L. Ju, Z. Wang, G.J. Zhao, Q. Dong, Laser Phys. **18**, 1501 (2008)
11. B.Q. Yao, X.M. Duan, L.L. Zheng, Y.L. Ju, Y.Z. Wang, G.J. Zhao, Q. Dong, Opt. Express **16**, 14668 (2008)
12. D.Y. Shen, A. Abdolvand, L.J. Cooper, W.A. Clarkson, Appl. Phys. B **79**, 559 (2004)
13. V. Petrov, M.C. Pujol, X. Mateos, Ò. Silvestre, S. Rivier, M. Aguiló, R.M. Solé, J. Liu, U. Griebner, F. Díaz, Laser Photon. Rev. **1**, 179 (2007)
14. M.C. Pujol, M.A. Bursukova, F. Güell, X. Mateos, R. Solé, J. Gavaldà, M. Aguiló, J. Massons, F. Díaz, P. Klopp, U. Griebner, V. Petrov, Phys. Rev. B **65**, 165121–1 (2002)
15. X. Mateos, V. Petrov, J. Liu, M.C. Pujol, U. Griebner, M. Aguiló, F. Díaz, M. Galan, G. Viera, IEEE J. Quantum Electron. **42**, 1008 (2006)
16. R. Solé, V. Nikolov, X. Ruiz, J. Gavaldà, X. Solans, M. Aguiló, F. Díaz, J. Cryst. Growth **169**, 600 (1996)
17. R. Solé, Ò. Silvestre, J. Massons, J. Gavaldà, M. Aguiló, F. Díaz, J. Cryst. Growth **310**, 1167 (2008)
18. M.C. Pujol, X. Mateos, A. Aznar, X. Solans, S. Suriñac, J. Massons, F. Díaz, M. Aguiló, J. Appl. Cryst. **39**, 230 (2006)
19. J. Rodriguez-Carvajal, *An Introduction to the Program Full Prof 2000* (Laboratorie Léon Brillouin CEA-CNRS Saclay, France, 2001)
20. R.D. Shannon, Acta Cryst. A **32**, 751 (1976)
21. M.C. Pujol, J. Massons, M. Aguiló, F. Díaz, M. Rico, C. Zaldo, IEEE J. Quantum Electron. **38**, 93 (2002)
22. S.A. Payne, L.L. Chase, L.K. Smith, W.L. Kway, W.F. Kruple, IEEE J. Quantum Electron. **28**, 2619 (1992)
23. M. Segura, M. Kadankov, X. Mateos, M.C. Pujol, J.J. Carvajal, M. Aguiló, F. Díaz, U. Griebner, V. Petrov, Laser Phys. Lett. **9**, 104 (2011)
24. X. Mateos, V. Jambunathan, M.C. Pujol, J.J. Carvajal, F. Díaz, M. Aguiló, U. Griebner, V. Petrov, Opt. Express **18**, 20793 (2010)